RESEARCH ARTICLE

Key Points:
- Major contribution for annual anomaly comes from the enhanced plasma densities in southern summer hemisphere during both daytime and nighttime
- Large offset between subsolar point and magnetic equator is responsible for southern low-latitude density enhancements during December
- The effective upward/downward neutral wind due to geomagnetic field geometry is the key factor for annual anomaly at daytime and nighttime

Correspondence to:
S. Tulasi Ram,
tulasi@iigs.iigm.res.in

Ionospheric annual anomaly—New insights to the physical mechanisms

V. Sai Gowtam[1] (iD) and S. Tulasi Ram[1] (iD)

[1]Indian Institute of Geomagnetism, Navi Mumbai, India

Abstract The ionospheric annual anomaly or nonseasonal anomaly of the ionosphere is characterized by globally increased ionization in December solstice than in June solstice. Though this phenomenon was reported several decades ago, the causal mechanisms have not been fully understood till today. In this paper, the F_2 layer peak electron density (N_mF_2) data from Formosa satellite 3/Constellation Observing System for Meteorology, Ionosphere, and Climate-radio occultation observations during the low solar activity year 2009 were systematically analyzed to investigate the physical mechanisms responsible for annual anomaly and its local time, latitudinal, and longitudinal variability. It is found that the annual anomaly is primarily dominant at Southern Hemisphere at all local times, with significant enhancements at equatorial ionization anomaly crest latitudes during noon to afternoon hours and at high latitudes during nighttimes. The annual anomaly in Northern Hemisphere occurs with relatively smaller magnitudes and confined only to morning to early afternoon hours (08–14 LT). This study brings out the important roles of effective neutral winds due to the geomagnetic field configuration and the offset between geomagnetic equator and subsolar point for the enhanced plasma density in the Southern Hemisphere during December that majorly contributes to the ionospheric annual anomaly. These results provide new insights to the responsible mechanisms behind the ionospheric annual anomaly and its local time latitudinal, and longitudinal variation

Plain Language Summary Ionospheric annual anomaly, characterized by globally enhanced ion densities during December than during June, is one of the unresolved problems of ionospheric physics since its discovery several decades ago. In this paper, the important role of thermospheric neutral winds for the ionospheric annual anomaly is discussed in detail. This study provides better insights to the causative physical mechanisms for the ionospheric annual anomaly.

1. Introduction

In ionospheric studies, the term "anomaly" is usually referred to the inconsistency of the F_2 layer electron density distribution with the Chapman theory of photoionization. In fact, the Chapman theory can explain the behavior of D, E, and F_1 layers of ionosphere. However, being that the transport processes are more important than chemical loss, F_2 layer is different from the other regions of ionosphere. Plasma transport processes due to E × B drifts and thermospheric winds can significantly alter the electron density distribution in the F_2 layer. Four types of anomalies, namely, equatorial ionization anomaly, winter or seasonal anomaly, semiannual anomaly, and annual anomaly or nonseasonal anomaly, are often found in the F_2 layer. One of the well-known anomalies of the equatorial ionosphere is the equatorial ionization anomaly (EIA) with its two maxima at off equatorial latitudes and minima at the dip equator. Detailed studies of EIA and its diurnal, seasonal and solar cycle variability in the latitudinal and altitudinal patterns using ionosondes, topside sounders, GPS-TEC data, and radio occultation measurements can be found in the literature [*Rajaram*, 1977; *Moffet*, 1979; *Anderson*, 1981; *Walker*, 1981; *Raghavarao et al.*, 1988; *Sharma and Raghavarao*, 1989; *Abdu et al.*, 1990; *Rastogi and Klobuchar*, 1990; *Stening*, 1992; *Walker et al.*, 1994; *Bailey et al.*, 1997; *Rishbeth*, 2000; *Sagawa et al.*, 2005; *Immel et al.*, 2006; *Lin et al.*, 2007a, 2007b; *Tulasi Ram et al.*, 2009; *Balan et al.*, 2013]. The second one is winter anomaly, characterized by the higher daytime N_mF_2 values in winter hemisphere than its conjugate summer hemisphere during solstices [*Rishbeth and Setty*, 1961; *Johnson*, 1964; *Torr and Torr*, 1973; *Zhao et al.*, 2007]. *Torr and Torr* [1973] and *Burns et al.* [2014] have shown that the winter anomaly is stronger in the Northern Hemisphere than in the Southern Hemisphere. The third anomaly is semiannual anomaly, in which the N_mF_2 values during equinoxes are much larger than solstices [*Volland*, 1969; *Mayr and Mahajan*, 1971; *Millward et al.*, 1996; *Balan et al.*, 2000; *Ma et al.*, 2003; *Li and Yu*, 2003]. Further, it is also reported that the ionization among the two equinoxes exhibits an asymmetry with higher plasma densities in

March equinox than in September equinox [*L. Liu et al.*, 2010]. The fourth is the annual anomaly or nonseasonal anomaly, in which, in the world as a whole, N_mF_2 values during December solstices are significantly greater than those in June solstices globally. Apart from these anomalies, recent studies also show that the nighttime midlatitude ionosphere often exhibits anomalous enhancements in the summer hemisphere, known as midlatitude summer nighttime anomaly (MSNA) [e.g., *Thampi et al.*, 2009; *H. Liu et al.*, 2010] in the northern hemispheric summer and Weddell Sea Anomaly (WSA) [e.g., *Bellchambers and Piggott*, 1958; *He et al.*, 2009; *Chen et al.*, 2011] in the southern hemispheric summer.

The ionospheric annual anomaly was first observed and reported by *Berkner and Wells* [1938]. Later, several studies on the annual anomaly have been carried out using the N_mF_2 data from paired ionosonde stations at nearly conjugate locations in Northern and Southern Hemispheres [*Yonezawa*, 1971; *Rishbeth and Muller-Wodarg*, 2006], the total electron content (TEC) data from a worldwide network of GPS stations [*Mendillo et al.*, 2005], topside ionospheric observations [*Su et al.*, 1998; *Liu et al.*, 2007] and Global N_mF_2 data from Constellation Observing System for Meteorology, Ionosphere and Climate (COSMIC) radio occultation observations [*Zeng et al.*, 2008]. These studies demonstrated that the annual anomaly exhibits significant local time and longitudinal and solar activity variations providing some important insights on the responsible mechanisms. *Rishbeth and Muller-Wodarg* [2006] employed the Coupled Thermosphere-Ionosphere-Plasmasphere (CTIP) model to study the annual anomaly. However, their CTIP simulations show a much smaller annual anomaly than was originally observed, which they speculatively attributed to dynamical influences of the tides of lower atmospheric origin. *Liu et al*. [2007] have investigated the annual anomaly in the topside ionosphere (~840 km) and shown that the changes in atomic oxygen concentration [O] can partially explain the annual anomaly using Naval Research Laboratory Mass Spectrometer and Incoherent Scatter Radar Exosphere (NRLMSISE-00) model. *Zeng et al*. [2008] studied the annual anomaly by using Formosa satellite 3 (Formosat-3)/COSMIC radio occultation (RO) measurements during 2006. They found that annual asymmetry index maximizes during local noon and midnight with a significant longitudinal variability. From the case-controlled model simulations using Thermosphere-Ionosphere Electrodynamics General Circulation Model, *Zeng et al*. [2008] have identified that the important factors that are responsible for ionospheric annual anomaly are the solstice difference of Sun-Earth distance, offset between geomagnetic and geographic center, tilt of geomagnetic dipole axis, and only a minor contribution from atmospheric tides of lower atmospheric origin. However, the detailed physical mechanisms about how the above factors contribute to the annual anomaly are still missing.

The interaction between vertical electrodynamic (E × B) drift and field-aligned transport due to neutral winds often causes hemispheric asymmetry in the equatorial ionization anomaly (EIA) during solstices with enhanced plasma density in the respective summer hemisphere during afternoon to midnight hours [*Lin et al*., 2007a and *Tulasi Ram et al*., 2009]. With the recent advancements in understanding the summer hemispheric enhancements due to hemispheric asymmetry of EIA during daytime and midlatitude enhancements (MSNA and WSA) during nighttimes via electrodynamic and wind-driven field-aligned transport processes, the physical processes involved in the unresolved ionospheric annual anomaly are revisited in this paper in connection with the above phenomena. In the present study, the important processes that are responsible for the annual anomaly and its local time, latitudinal, and longitudinal variations are investigated using the global radio occultation observations from Formosat-3/COSMIC during a low solar activity year 2009. The data selected for this study are briefly described in section 2; the ionospheric annual anomaly in F_2 layer peak electron density (N_mF_2) and its local time, latitudinal, and longitudinal variations are presented in section 3; the responsible mechanisms in terms of electrodynamic drifts and wind-driven transport processes are discussed in detail in section 4, and the important conclusions are briefly summarized in section 5.

2. Data

The FORMOSAT-3/COSMIC, a Taiwan-United States joint mission, primarily dedicated to radio occultation experiment to study the Earth's atmosphere and ionosphere. COSMIC is a constellation of six microsatellites, orbiting at an altitude of ~800 km in 72° inclined circular orbits. COSMIC-retrieved ionospheric profiles are in good agreement with the ground-based ionosonde and Radar electron density profiles [*Schreiner et al*., 2007; *Lei et al*., 2007]. In the present study, we used COSMIC data during 2009 provided by the University Corporation for Atmospheric Research (UCAR) COSMIC Data Analysis and Archival Center
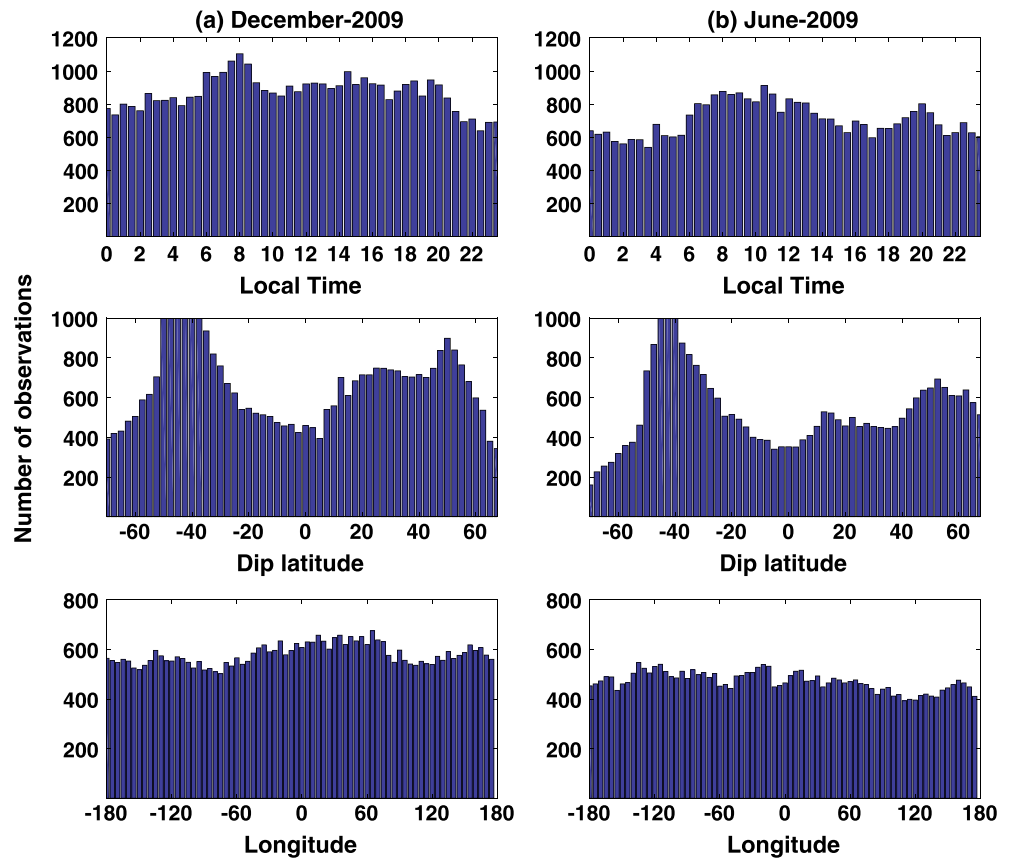
Figure 1. The local time (top row), dip latitude (middle row), and geographic longitude (bottom row) coverage of Formosat-3/COSMIC RO observations during the 41 day periods of (a) December and (b) June solstices.

(CDAAC) (http://www.cosmic.ucar.edu). All COSMIC data observations under quiet geomagnetic conditions with Kp index less than 3 are used to avoid the anomalous changes in ionosphere during geomagnetically disturbed periods. Also, the bad profiles with a standard deviation value that is greater than 1.5 are discarded following the method by *Yang et al.* [2009]. Nearly 2000 electron density profiles per day provide a high spatial and temporal resolution to study the ionosphere. In the present study, the 41 day period that centered on 21 June and 21 December is considered to represent the June and December solstices, respectively. The 41 day mean $F_{10.7}$ solar flux values of June and December solstices are 70.94 and 74.87 solar flux unit (sfu) (1 sfu = 10^{-22} W m^{-2} Hz^{-1}), respectively, which are nearly comparable, hence, best suitable for comparison excluding the solar cycle effects (between June and December periods in an ascending phase of solar cycle). The 41 day period data from COSMIC during both June and December solstices provide good spatial and temporal coverage. For example, Figure 1 shows the coverage of COSMIC RO observations every 30 min local time (top row), 2.5° dip latitude (middle row), and 5° geographic longitude (bottom row) bins during the December (Figure 1a) and June solstices (Figure 1b).

3. Results

The F_2 layer peak electron density (N_mF_2) values from Formosat-3/COSMIC vertical electron density profiles during both June and December solstice periods were binned into 2.5° magnetic dip latitude and 30 min local time bins. Within each dip latitude and local time grid, the N_mF_2 values that correspond to different longitudes are averaged and the zonal mean N_mF_2 values are computed. Further, a five-point moving average is applied in both dip latitude and local time directions, and the smoothed zonal mean N_mF_2 variation as a function of magnetic dip latitude and local time for both June and December solstices of the year 2009 are shown in Figures 2a and 2b, respectively. During the June (December) solstices, the Northern
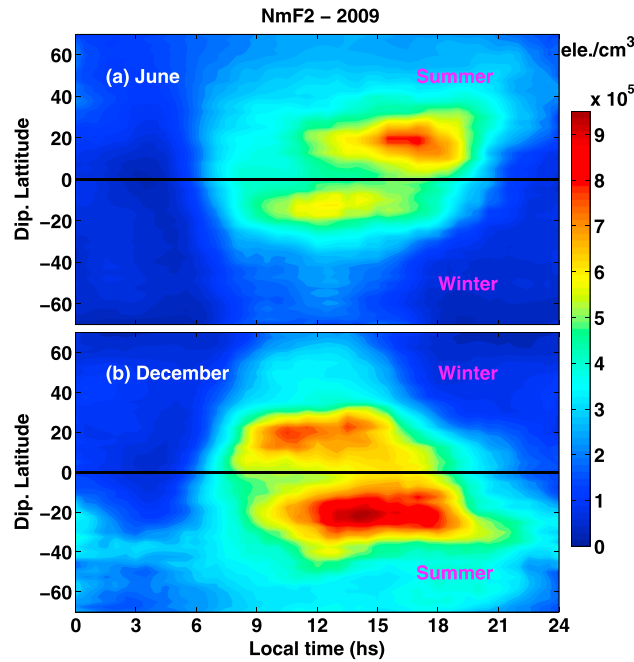
Figure 2. Local time and magnetic dip latitudinal variation of the zonally averaged N_mF_2 during (a) June and (b) December solstices of the year 2009. Solid black horizontal line represents the dip equator.

Hemisphere will be the summer (winter) and the Southern Hemisphere is winter (summer). The respective summer and winter hemispheres during the June and December solstices are indicated in Figures 2a and 2b.

A double-crest equatorial ionization anomaly (EIA) structure with a trough at the dip equator can be clearly seen during daytime in both the solstices. A careful examination reveals that the EIA crests in the respective winter hemispheres are stronger from morning to noon hours (say ~0800 to ~1200 LT) during both the solstices. However, at later local times, the EIA crests in the respective summer hemispheres become much stronger than those in the winter hemispheres during both the solstices. The larger N_mF_2 values in the summer hemisphere are further maintained throughout from afternoon to predawn hours. Interestingly, at middle to high latitudes (>30° magnetic dip latitudes), the N_mF_2 values in their respective summer hemispheres are higher than those in winter hemisphere at all local times. This actually indicates the absence of winter anomaly at midlatitudes during this low solar activity year 2009. Similar results were consistently observed throughout the ascending phase of solar cycle 24 from 2008 to 2012 from the Formosat-3/COSMIC N_mF_2 data, presented elsewhere [*Sai Gowtam and Tulasi Ram*, 2017]. Using the harmonic analysis of COSMIC radio occultation data during 2006–2008, *Liu et al.* [2009] have shown the similar hemispheric asymmetry in both N_mF_2 and topside electron densities. Further, *Liu et al.* [2009] have shown that the winter/seasonal anomaly exists only at lower altitudes and gradually disappears at higher altitudes. Recently, *Burns et al.* [2014] have also shown that the winter anomaly does not occur during the low solar activity periods with the $F_{10.7}$ solar flux below 90–100 × 10^{-22} W m^{-2} Hz^{-1}.

Further, the comparison of N_mF_2 between June (Figure 2a) and December (Figure 2b) solstices clearly shows that the overall ionization (N_mF_2) in December solstice is significantly higher than in June solstice clearly indicating the ionospheric annual anomaly. Ionospheric annual anomaly is generally studied using the observations from magnetically conjugate locations [e.g., *Yonezawa*, 1971; *Rishbeth and Muller-Wodarg*, 2006] in order to avoid the effects of winter anomaly. *Rishbeth and Muller-Wodarg* [2006] suggested annual anomaly index (AI) to quantifying the strength of annual anomaly as

$$AI = \frac{N_mF_{2NS}\,(Dec) - N_mF_{2NS}\,(Jun)}{N_mF_{2NS}\,(Dec) + N_mF_{2NS}\,(Jun)} \qquad (1)$$

where

$$N_mF_{2NS}\,(\theta, \lambda) = \frac{1}{2}.[N_mF_2(\theta_N, \lambda) + N_mF_2(\theta_S, \lambda)] \qquad (2)$$

and θ is the magnetic dip latitude and λ is the geographic longitude. The subscripts N and S in equations (1) and (2) represent the northern and southern hemispheric conjugate latitudes, respectively. The positive AI indicates occurrence of ionospheric annual anomaly with higher December N_mF_2 values than in June. As an example, the value of 0.2 for AI indicates that the ionization in December is 50% higher than in June. The annual anomaly index (AI) is computed using equations (1) and (2) at 2.5° dip latitude and 30 min local time bins. Figure 3a presents the zonally (longitudinally) averaged AI as a function of local time and dip
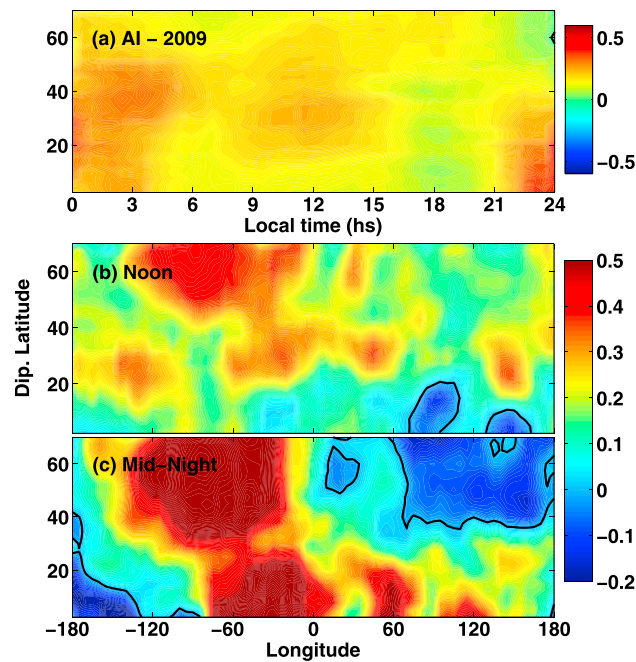
Figure 3. (a) Local time and magnetic dip latitudinal variation of zonally averaged AI during 2009. (b, c) Variations of AI as function of longitude and magnetic dip latitudes during noon and midnight hours, respectively. Positive (negative) AI values indicate that N_mF_2 values in December solstices are greater (smaller) than in June solstices. Solid black curve indicates the zero contour level.

latitude. It can be observed from this figure that the AI is positive at all local times indicating the occurrence of annual anomaly. Further, the AI is generally intense around local noon and midnight hours and relatively weaker around dawn and dusk periods. The increase in AI around noon hours can be seen at low to midlatitudes (15–50°), and the higher AI values around midnight occur starting from the equatorial latitudes.

It should be noted that the variations of AI shown in Figure 3a were longitudinally averaged AI values; hence, the longitudinal variability in the annual anomaly cannot be observed. The question whether the observed noon and midnight enhancements in AI correspond to global or to a specific longitude sector cannot be resolved from Figure 3a. Therefore, with a view to further examine the detailed latitudinal and longitudinal distributions of AI, the N_mF_2 values that correspond to noon (between 11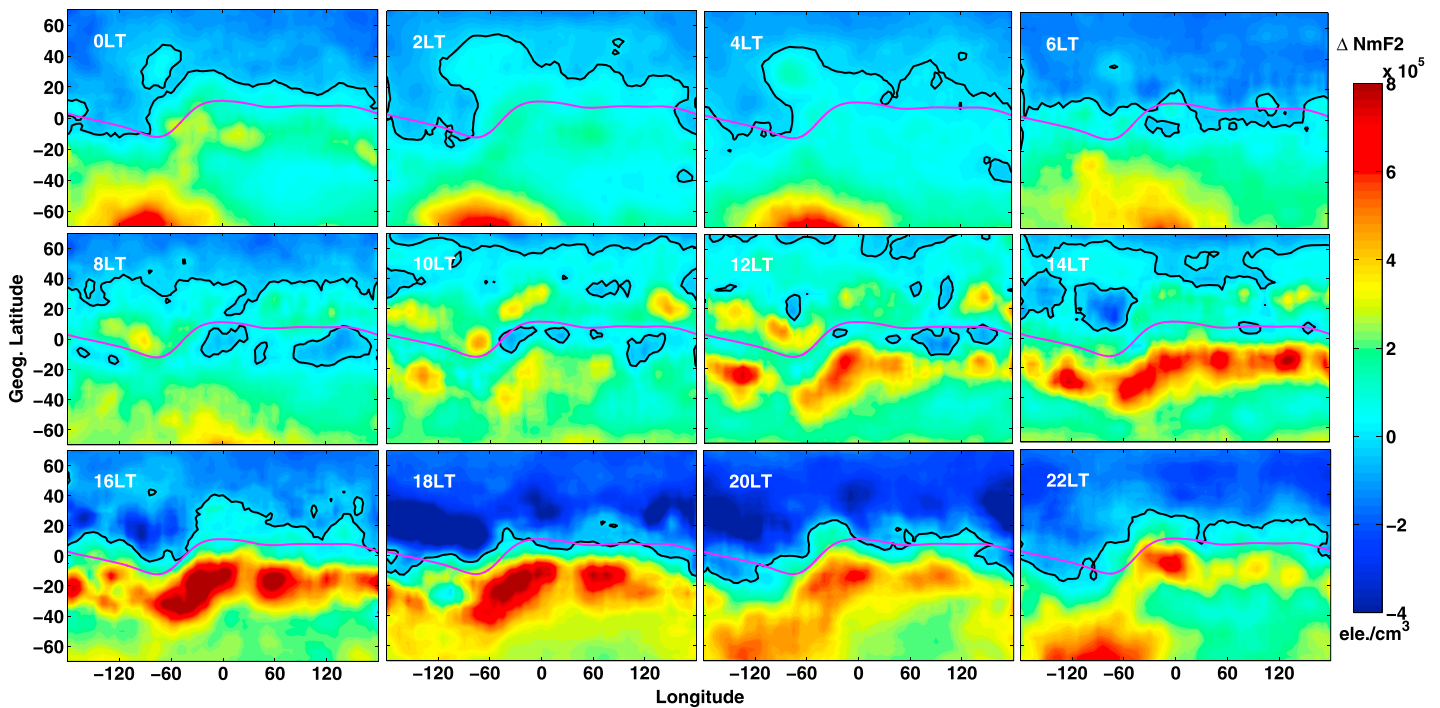30 and 1230 LT) and midnight (between 2330 and 0030 LT) periods were gridded into 2.5° magnetic dip latitude and 5° longitude grids. Then the longitudinal and magnetic dip latitudinal variation of AI is computed using equations (1) and (2). Figures 3b and 3c show the longitudinal and latitudinal variations of AI during noon and midnight periods, respectively. The solid black curves in Figures 3a and 3b represent the zero AI contour level. During noon (Figure 3b), the AI exhibits overall positive values at all longitudes except small equatorial regions centered at ~80°E and 150°E longitudes. Further, the longitudinal variation of AI shows broad enhancements around ~150°W–110°W, ~60°W–50°E, and ~130°E–150°E longitudes of low latitude to midlatitude (20°–40°). Another strong enhancement can be observed at high latitudes (~50°–70° dip latitude) of western longitudes from ~120°W to 20°W. During midnight hours (Figure 3c), this high-latitude enhancement at western longitudes is further intensified and extended equatorward up to ~35° latitude. Also, the AI during nighttimes exhibits significant enhancements at equatorial and low latitudes over the longitudes from 80°W to 150°E. Further, the AI is negative at middle and high latitudes of 50°E–180°E longitudes and also around low latitudes of 180°W to 120°W longitudes. The global mean values of AI during noon and midnight periods are 0.1997 and 0.2255 indicating that the global mean N_mF_2 in December are ~50% and ~58% higher than in June during noon and midnight periods, respectively.

Therefore, from the results presented in Figures 2 and 3, one can conclude that the ionospheric annual anomaly occurs at all local times with broad enhancements around noon and midnight periods (Figures 2 and 3a). Further, the annual anomaly index (AI) exhibits significant latitude and longitudinal variability during both noon and midnight hours (Figures 3b and 3c). It should be noted that the anomaly index (AI) presented in Figure 3 is computed using equations (1) and (2) which averages the N_mF_2 values at conjugate latitudes from Northern and Southern Hemispheres. Averaging of N_mF_2 values from conjugate southern and northern latitudes minimizes the summer and winter differences in the respective hemispheres and also removes the effects of winter anomaly. As a result, equation (1) brings out the quantitative estimate of ionospheric annual anomaly as the difference between December and June solstices.

However, by averaging the conjugate latitude N_mF_2 values while computing AI, one cannot observe the magnitude differences of annual anomaly in Northern and Southern Hemispheres. In other words,

Figure 4. Geographic longitudinal and latitudinal variations of N_mF_2 difference between December and June solstices ($\Delta N_mF_2 = N_mF_{2\text{Dec}} - N_mF_{2\text{Jun}}$) without combining the opposite hemispheres every 2 h local time intervals centered on the time shown in respective panels. Solid black curve indicates the zero contour level.

whether the strength of ionospheric annual anomaly is equal in both hemispheres or there is any hemispheric dominance cannot be resolved from AI computed using equations (1) and (2). Therefore, with a view to examine the relative contributions from Northern and Southern Hemispheres to the annual anomaly, the difference in N_mF_2 between December and June solstices ($\Delta N_mF_2 = N_mF_{2\text{Dec}} - N_mF_{2\text{Jun}}$) is computed without combining the opposite hemispheres. Figure 4 shows the two-dimensional longitudinal and latitudinal distributions of ΔN_mF_2 every 2 h local time intervals from 00 LT to 22 LT. The ΔN_mF_2 variations presented in each panel represent an average of ±1 h LT interval centered on the time shown in the respective panels. The positive (negative) values indicate the higher (smaller) values of N_mF_2 in December than in June. The black curves represent the zero contour level. It can be observed from this figure that the Southern Hemisphere shows large positive values of ΔN_mF_2 at all local times. During noon to afternoon hours (1200 to 1800 LT), the ΔN_mF_2 values are significantly large at southern EIA crest latitudes. These higher ΔN_mF_2 values at southern EIA crest latitudes persisted up to midnight around 60°W to 150°E longitudes. During nighttimes (2000 to 0600 LT), the ΔN_mF_2 exhibits substantial enhancements at southern high latitudes around 150°W to 60°W longitudes. On the other hand in the Northern Hemisphere, the ΔN_mF_2 is negative (N_mF_2 in December is smaller than in June) during most local times, i.e., from 00 to 06 LT and 1600 to 2200 LT. Only during the production dominant hours of 10–14 LT, the ΔN_mF_2 is slightly positive in Northern Hemisphere and the positive values are confined only to northern low-latitudes at 08 LT. Further, one important observation from the ΔN_mF_2 variations presented in Figure 4 is that the positive ΔN_mF_2 values in Southern Hemisphere are generally much stronger (higher magnitudes) than the negative ΔN_mF_2 in the Northern Hemisphere. This suggests that the ionization (N_mF_2) in December is substantially larger than that in June. Therefore, the results presented in Figures 3 and 4 clearly indicate that the ionospheric annual anomaly (and the positive AI values) primarily comes from the southern (summer) hemisphere, with a smaller contribution from the Northern Hemisphere during the production dominant morning (0800 LT) to early afternoon (1400 LT) hours. *Liu et al.* [2007, 2009] have also shown that annual variation in N_mF_2 is significantly stronger in Southern Hemisphere. Similar enhancements in southern (summer) hemisphere were also observed at different altitudes including topside ionosphere, reported by *Sai Gowtam and Tulasi Ram* [2017].

However, they have not discussed the responsible mechanisms which will be addressed in detail in the present paper.

4. Discussion

The important insights about ionospheric annual anomaly drawn from the results presented in Figures 2–4 are as follows: (i) the annual anomaly primarily occurs in the Southern Hemisphere at all local times, (ii) the annual anomaly is significantly enhanced at southern EIA crest latitudes during noon to afternoon hours suggesting its close relationship with the enhanced EIA crests in the summer hemisphere during December, (iii) the annual anomaly during nighttimes exhibits significant enhancements at southern high latitudes around 150°W to 60°W indicating the role of Weddell Sea Anomaly (WSA) region, and (iv) the annual anomaly in the Northern Hemisphere occurs with relatively smaller magnitudes only during the production dominant hours of 0800 to 1400 LT and is mostly absent at other local times. These results bring out the importance of Southern Hemisphere contribution to the annual anomaly during both daytime and nighttime. The possible mechanisms responsible for the above observations are discussed in the following sections.

Several physical processes contribute to the observed annual anomaly and its local time, latitudinal, and longitudinal variability. The positive ΔN_mF_2 values in both hemispheres during the morning to early afternoon hours (08–14 LT) (Figure 4) suggest that the varying Sun-Earth distance between December and June solstices is one of the important factors, particularly, during daytime when the production is dominant. The annual variation of ~3.5% in Sun-Earth distance (0.983 AU for December and 1.017 AU for June) can account for ~7% higher solar EUV radiation during December than in June that contributes to the annual anomaly. *Zeng et al.* [2008] have demonstrated through model simulations that the varying Sun-Earth distance between December and June solstice can account for about 7% of annual asymmetry. In addition to the varying Sun-Earth distance, the neutral and electrodynamic processes in the presence of geomagnetic field configuration play important roles in strengthening the southern EIA crests in December and thus majorly contributing to the annual asymmetry during noon to afternoon hours.

4.1. Interplay Between Transequatorial Neutral Wind and Equatorial Fountain Process

During solstices, the thermospheric neutral wind blows across the equator from summer hemisphere to winter hemisphere. This summer to winter transequatorial wind causes field-aligned transport of plasma upward/equatorward in the summer hemisphere and downward/poleward in the winter hemisphere due to finite inclination of geomagnetic field lines. Another important electrodynamic process that operates during daytime is the equatorial fountain due to enhanced eastward zonal electric field at the equator. The plasma over the geomagnetic equator is uplifted via E × B drift which diffusively settles at low latitudes on both sides of the equator under the gravity and pressure gradient forces. In the summer hemisphere, the field-aligned plasma transport due to neutral wind and equatorial fountain process is in opposite direction, whereas the plasma transport due to the two processes is in the same direction in winter hemisphere. Thus, the N_mF_2 values at low-latitude region of both summer and winter hemispheres are largely controlled by the relative strengths of transequatorial neutral wind and equatorial fountain process. During morning period, the transequatorial neutral wind is dominant and causes interhemispheric transport of plasma along the field lines to the winter hemisphere. This leads to higher N_mF_2 values in the winter hemisphere (Figure 2). However, the zonal electric field maximizes and equatorial fountain process reaches its maximum strength around noon. The intensified fountain process impedes the interhemispheric plasma transport by neutral winds. In summer hemisphere, the upward/equatorward field-aligned transport by neutral winds is counteracted by the equatorial fountain process causing formation of stronger EIA crests at relatively higher altitudes around noon to early afternoon hours. On the other hand, the downward/poleward field-aligned transport by neutral winds is augmented by the equatorial fountain process causing weak EIA crests and smaller N_mF_2 values in the winter hemisphere. This transition of higher N_mF_2 values from winter to summer hemisphere usually occurs around noon when the equatorial fountain process becomes stronger (Figure 2). It should be noted that the results drawn from Figure 2 correspond to asymmetry in the zonal (longitudinal) mean in N_mF_2, discounting the longitudinal variability, for simplicity.

This diurnal variation in the hemispheric asymmetry of EIA has significant effects on annual anomaly. For example, Figure 5 shows the latitudinal and altitudinal distribution of electron density during the
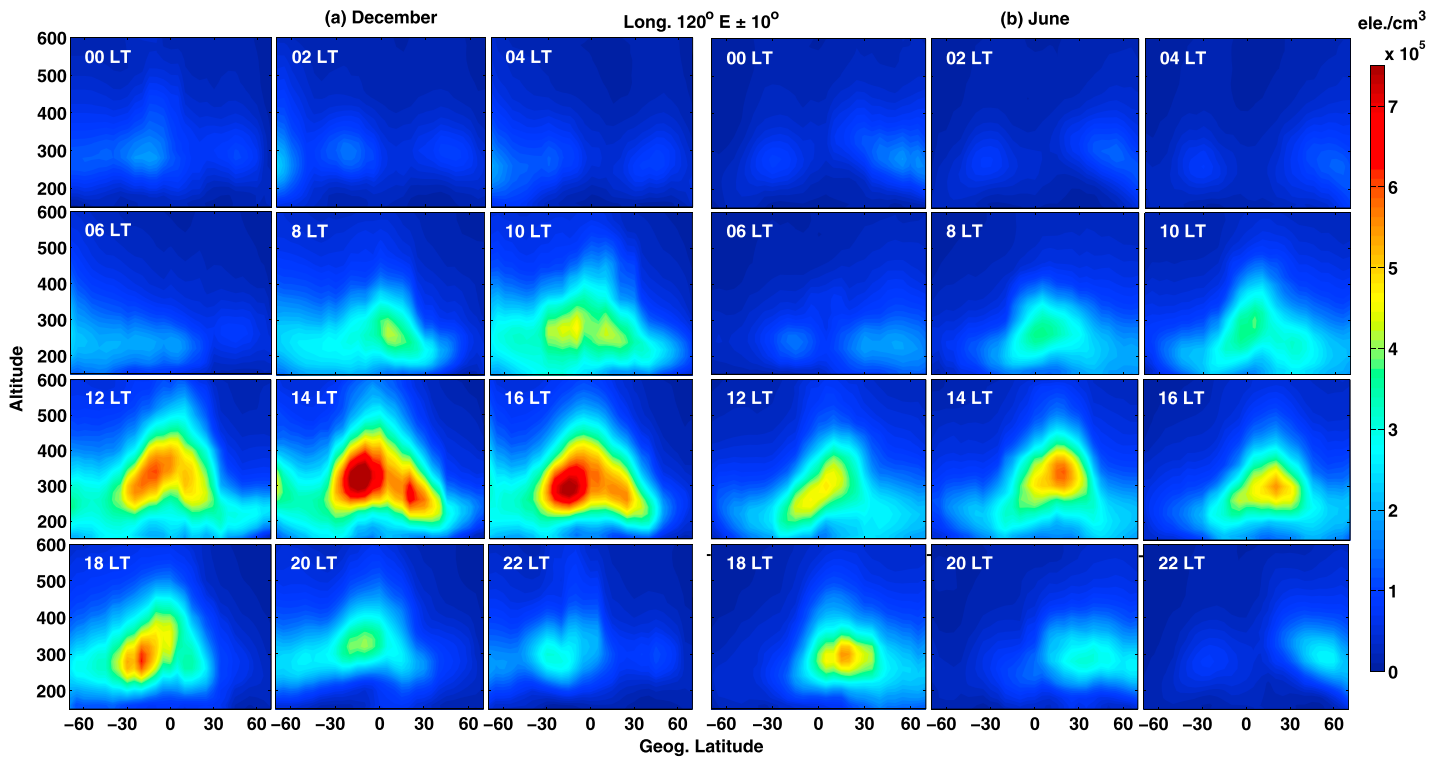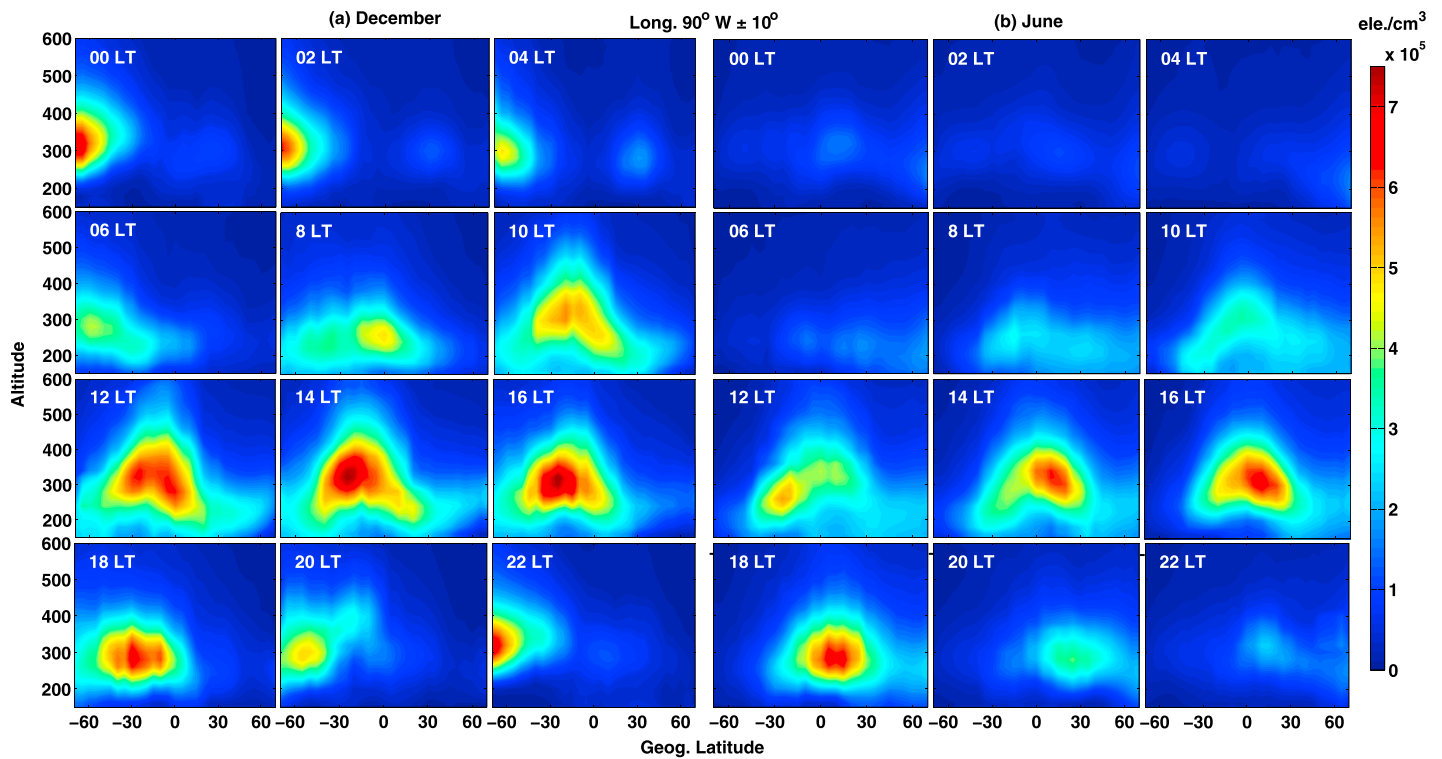
Figure 5. Latitudinal and altitudinal distribution of electron density during the (a) December and (b) June solstices every 2 h local time intervals along the 120°E (±10°) longitudinal sector.

December (Figure 5a) and June (Figure 5b) solstices every 2 h local time intervals along the 120°E (±10°) longitudinal sector. It can be observed that during December solstices (Figure 5a), the ionization starts building in the summer (southern) hemisphere at 6 LT because of early sunrise in the summer hemisphere. However, the plasma density in the winter (northern) low latitudes becomes stronger than that in summer hemisphere at 8 LT, probably, due to interhemispheric plasma transport by dominant transequatorial neutral winds. At 10 LT, the EIA crest in summer hemisphere is intensified and becomes nearly equal to winter hemisphere due to impeding interhemispheric plasma transport by counteracting equatorial fountain process. Around noon (12 LT), the EIA crest in summer (southern) hemisphere becomes stronger and elevated to higher altitudes than in winter hemisphere because of the interplay between neutral winds and dominant equatorial fountain process acting in opposite direction in the summer hemisphere. The EIA crests in summer hemisphere are further intensified during the afternoon hours (14–16 LT). Also, the electron densities in the summer hemisphere remain to be higher and maintained at higher altitudes even after sunset (18 LT) and up to midnight, perhaps, assisted by the equatorward neutral wind. Similar diurnal variations in the hemispheric asymmetry of EIA can also be observed during the June solstices from Figure 5b. However, the transition of stronger EIA crests from winter to summer hemispheres occurred at 14 LT and the magnitudes of summer EIA crests are much stronger in December than in June solstice. The mechanisms responsible for this magnitude difference in summer EIA crests between December and June solstices are discussed in sections 4.2 and 4.3.

The comparison of electron density distributions between December (Figure 5a) and June (Figure 5b) clearly shows that the electron densities in Southern Hemisphere are significantly higher during December solstices than in June solstices. This annual anomaly is due to involvement of several physical mechanisms: First, the closer Sun-Earth distance during December compared to June solstices as discussed earlier, and second, the above discussed hemispheric asymmetry of EIA (due to the interplay between neutral winds and equatorial fountain process) gives not only the higher electron densities in the Southern Hemisphere during December but also the smaller densities during June around noon to afternoon hours. As a result, the Southern Hemisphere exhibits significantly large asymmetry between December and June solstices particularly at

Figure 6. Latitudinal and altitudinal distribution of electron density during the (a) December and (b) June solstices every 2 h local time intervals along the 90°W (±10°) longitudinal sector.

low to middle latitudes, which is the major contribution for annual anomaly during daytime. This is consistent with the observed strong enhancements in ΔN_mF_2 at southern low latitudes during noon to afternoon hours in Figure 4. Further, the higher electron densities in the southern low latitudes are maintained even after sunset and up to midnight during December (Figure 5a). In contrast, the electron density in the southern low latitudes is quickly recombined after sunset during June (Figure 5b) solstice. This is responsible for positive ΔN_mF_2 values observed at equatorial and southern low latitudes during nighttimes in Figure 4. Further, it is also interesting to observe higher electron densities at northern midlatitudes during nighttime (2000–0600 LT) in June solstice, which is responsible for negative values of ΔN_mF_2 in the Northern Hemisphere during nighttimes (Figure 4). This midlatitude enhancement in June solstice can be attributed to midlatitude summer nighttime anomaly (MSNA) reported by *Thampi et al.* [2009] and *H. Liu et al.* [2010] due to phase reversal of diurnal cycle.

Figure 6 shows the similar latitudinal and altitudinal distributions of electron density shown in Figure 5, however, for a longitudinal sector centered at 90°W. The latitudinal and altitudinal variations of electron density at equatorial and low latitudes during daytime are similar to those observed in Figure 5 during both December and June solstices. However, the interesting feature that can be observed in Figure 6a is the significantly higher electron densities at southern middle and high latitudes (40–70°S) during nighttimes in December solstices. Further, this nighttime density at high latitudes maximizes at midnight (00 LT) and significantly higher than its midday (12 LT) values. This nighttime high-latitude feature at the southern Pacific region during December solstices is widely known as Weddell Sea Anomaly (WSA) [*Bellchambers and Piggott*, 1958; *Penndorf*, 1965; *Dudeney and Piggot*, 1978; *Lin et al.* 2009; *He et al.* 2009]. The WSA at southern Pacific region is generally attributed to the combined effects of finite ion production at high latitudes, southward offset of geomagnetic equator with respect to geographic equator, eastward declination of field lines, and equatorward neutral wind [*He et al.* 2009; *Lin et al.* 2009]. Further, *Lin et al.* [2010] have shown that the WSA in southern Pacific region and MSNA in northern Asian and European regions are similar midlatitude nighttime features that exist in summer hemispheres at longitudes where the geomagnetic equator is located poleward of geographic equator. Later, *H. Liu et al.* [2010] have shown that these midlatitude nighttime enhancements
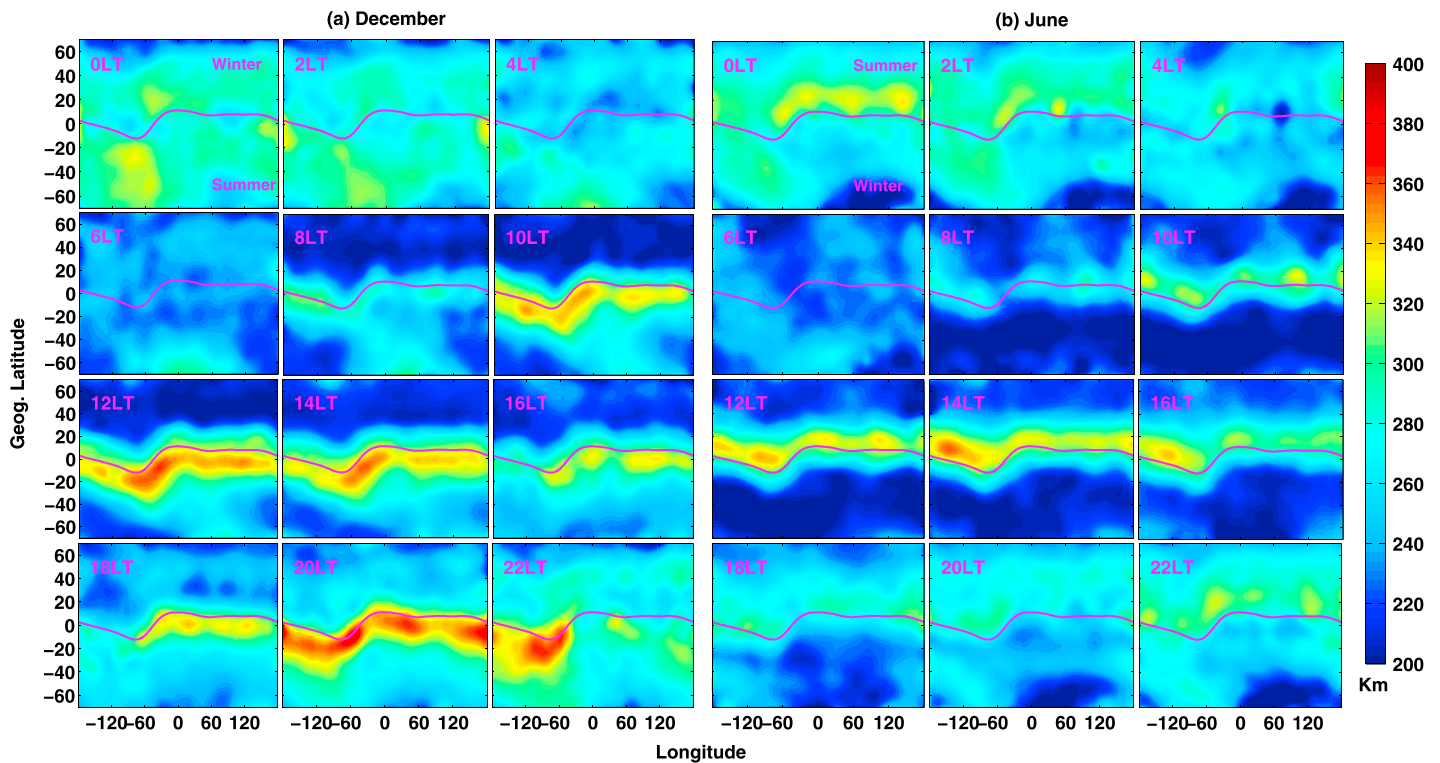
Figure 7. Longitudinal and latitudinal variations of h_mF_2 during the (a) December and (b) June solstices every 2 h local time interval.

(WSA and MSNA) are the part of reversed diurnal cycle which includes not only nighttime enhancement but also a noontime depletion mainly due to combined effects of geomagnetic field configuration and equatorward neutral winds. These enhanced nighttime densities due to WSA are responsible for enhanced ΔN_mF_2 values over 150°W to 60°W longitudes in the Southern Hemisphere shown in Figure 4.

The F_2 layer peak height (h_mF_2) generally reflects the dynamics of ionosphere due to the E × B drift and field-aligned plasma transport by the neutral winds. For example, Figure 7 shows the longitudinal and latitudinal variations of h_mF_2 during December (Figure 7a) and June (Figure 7b) at every 2 h local time interval. As discussed earlier the summer-to-winter hemispheric transequatorial neutral wind transports the plasma upward/equatorward in the summer hemisphere and downward/poleward in the winter hemisphere. Further, the interaction between transequatorial neutral winds and equatorial fountain process leads to the formation of EIA crests at relatively higher altitudes in the summer hemisphere than in the winter hemisphere. This can be clearly observed as significantly increased h_mF_2 at low latitudes in their respective summer hemispheres around 08–20 LT in December (Figure 7a) and around 08–18 LT in June (Figure 7b) solstices. The higher h_mF_2 values indicate the elevation of F_2 layer to higher altitudes leading to the formation of stronger EIA crests (due to reduced recombination loss) in the respective summer hemispheres as noted in Figures 5 and 6. The nighttime enhancements at summer hemispheric midlatitudes can also be observed in h_mF_2 around Weddell Sea Anomaly region during December (Figure 7a) and northern midlatitudes during June (Figure 7b). Another interesting observation from Figure 7 is that the low-latitude summer hemispheric h_mF_2 values are generally higher in December solstices (Figure 7a) than in June solstices (Figure 7b).

4.2. Offset Between Geomagnetic Equator and Subsolar Point

As discussed in section 4.1, the interplay between the transequatorial neutral winds and equatorial fountain process leads to stronger EIA crests in the respective summer hemisphere during both June and December solstices. However, during December, the effect of neutral winds appears to be more pronounced over large portion of globe where the geomagnetic equator is located over northern geographic latitudes. During December, the subsolar point located around ~23.5°S latitude creates the pressure bulge and drives interhemispheric wind toward northern latitudes. Due to significant inclination angle of field lines around subsolar

point, the northward wind can effectively uplift the plasma along the field lines and the counter action due to equatorial fountain process causes stronger EIA crests in the Southern Hemisphere during December solstices. On the other hand, the subsolar point during June (~23.5°N) is relatively closer to the geomagnetic equator and the inclination angle of field lines near subsolar point is relatively smaller. Hence, the upward push of plasma due to southward wind is relatively less effective during June at longitudes where the geomagnetic equator is located in northern geographic latitudes. This difference in the effectiveness of neutral winds between December and June solstices can be observed as the higher h_mF_2 values at southern low latitudes during December (Figure 7a) than at northern low latitudes of June (Figure 7b) over most longitudes. Therefore, the difference in the offset between subsolar point and geomagnetic equator causes relatively higher h_mF_2 values and stronger EIA crests in southern summer (December) than in northern summer (June) (Figure 5) thereby contributing to the annual anomaly, particularly during noon to afternoon hours at low latitudes. The same mechanism could produce higher h_mF_2 values and stronger EIA crests in northern summer (June) around the longitudes where the geomagnetic equator is located at southern geographic latitudes. One can observe that the northern EIA crests are stronger at 90°W longitude (Figure 6b) (where the geomagnetic equator is displaced to southern geographic latitudes) compared to 120°E longitude (Figure 5b). This causes strong negative ΔN_mF_2 values in northern low latitudes as seen from Figure 4 during 1400–1800 LT at these longitudes. However, the plasma density in Southern Hemisphere is still slightly higher in December than in June in this sector, probably, due to other factors such as Sun-Earth distance and westward zonal wind in the presence of large declination angles of field lines as discussed in the following section.

4.3. Effective Neutral Wind—HWM Model Simulation

In addition to the transequatorial meridional winds, the zonal winds also can play significant role in F region plasma transport where the magnetic declination angle is significant. For example, at Brazilian longitudes where the declination angle of field lines is largely westward, the westward zonal wind during daytime causes upward field-aligned transport of plasma leading to the enhanced ionization in the southern magnetic low latitudes. Similarly, the westward wind causes downward push of plasma leading to plasma density reduction in northern magnetic low latitudes. With a view to examine the combined effects of zonal and meridional neutral winds on the plasma transport, the effective wind that can cause upward/downward transport of plasma along field lines is computed following the equation given by *Titheridge* [1995] as

$$W_{\text{eff}} = (MW \cos D \pm ZW \sin D) \cos I \sin I \quad (3)$$

where MW and ZW are meridional (equatorward positive) and zonal (eastward positive) winds, respectively. Here + and – signs apply in the Southern and Northern Hemispheres. Here the meridional and neutral winds are derived from Horizontal Wind Model (HWM-2014) [*Drob et al.* 2015] and magnetic inclination (I) and declination (D) angles are obtained from International Geomagnetic Reference Field Model—2011. The effective upward/downward wind is computed using (3) at every 10° longitude and 5° latitude intervals. For example, Figures 8a and 8b show the longitudinal and latitudinal variations of effective wind (W_{eff}) during December and June solstices, respectively, at local noon. The positive/negative values of W_{eff} indicate that the transport of plasma due to this effective wind is upward/downward; hence, in short, we refer it as upward/downward effective wind. This upward/downward effective wind can cause increase/decrease of plasma density due to reduced/increased loss due to recombination. In general, the effective wind variations presented in Figures 8a and 8b capture the h_mF_2 variations at 12 LT presented in Figures 7a and 7b, respectively. The effective wind at low latitudes is upward (downward) in their respective summer (winter) hemispheres during both June and December solstices because of summer to winter hemispheric wind. However, the upward effective wind around noon is relatively larger in southern summer hemisphere during December (Figure 8a) at longitudes where the geomagnetic equator is located in northern geographic latitudes as well as at longitudes with westward magnetic declination. Similar enhancement in upward W_{eff} can also be observed in northern low latitudes during June (Figure 8b) at longitudes where the geomagnetic equator is located in southern geographic latitudes and with eastward magnetic declination.

In southern low latitudes, the W_{eff} is not only largely upward during December but also downward during June causing large difference between December and June. This can also be seen as significantly large h_mF_2 values during December and small h_mF_2 values during June at southern low latitudes in Figures 7a and 7b. This difference explains the large difference in N_mF_2 values between December and June solstices
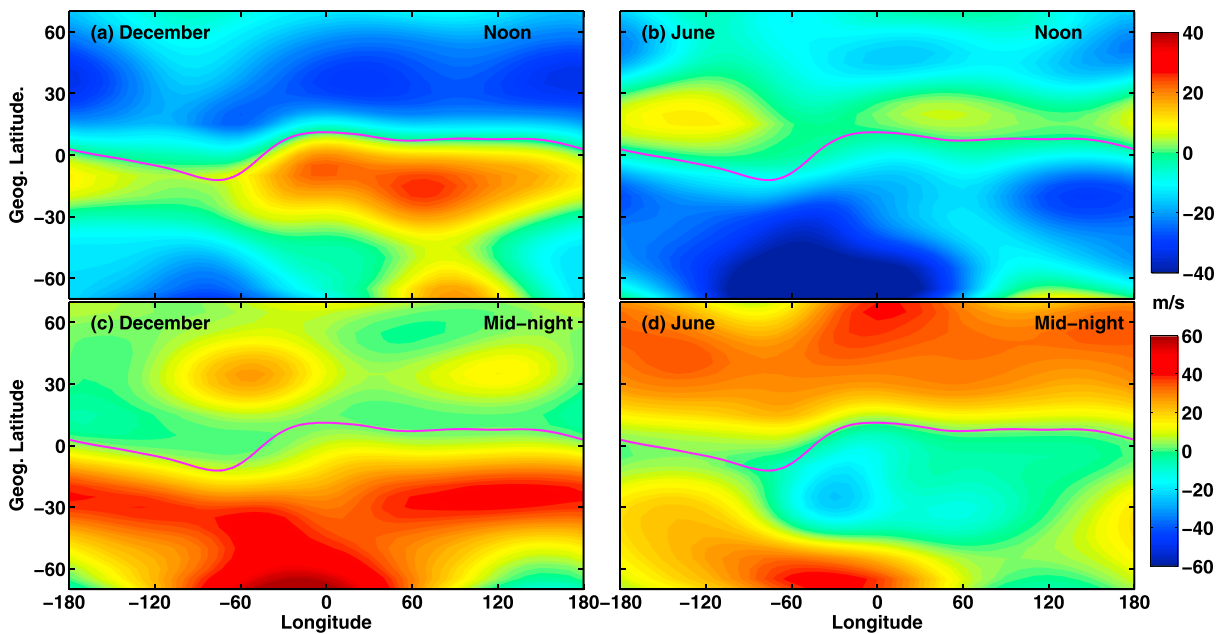
Figure 8. Geographic longitude and latitudinal variations of effective wind W_{eff} (upward positive) during (a, c) December and (b, d) June solstices at noon and midnight hours.

in the Southern Hemisphere, particularly at southern EIA crest latitudes as strong positive $\Delta N_m F_2$ values observed in Figure 4 during noon and afternoon hours. On the other hand, the upward W_{eff} in the northern low latitudes is relatively smaller during June (Figure 8b), hence, causing relatively smaller $h_m F_2$ values (Figure 7b) and weaker EIA crests when interacted with equatorial fountain process as observed from Figure 5b. The smaller positive $\Delta N_m F_2$ values around 08–14 LT in the Northern Hemisphere (Figure 4) would probably be due to these weaker EIA crests which more or less are compensated by the additional ionization by ~7% increase in solar EUV flux during December. Further, the higher O/N2 density ratio generally observed in December solstices than in June solstices in Northern Hemisphere [*Burns et al*. 2014] may also support the smaller positive $\Delta N_m F_2$ values observed at northern midlatitudes during the production dominant hours of 10–14 LT.

Figures 8c and 8d show the variations of W_{eff} during December and June solstices, respectively, during midnight hours. In the Northern Hemisphere, the W_{eff} is largely upward during June and very small during December. This large upward W_{eff} during June is responsible for enhanced nighttime densities (MSNA) [*Thampi et al*. 2009; *Lin et al*. 2010; *H. Liu et al*. 2010] and negative $\Delta N_m F_2$ values in the Northern Hemisphere during around midnight (Figure 4). In the Southern Hemisphere, the W_{eff} is relatively higher during December than in June solstice. This difference between December and June becomes more pronounced at southern high latitudes around WSA region causing large positive $\Delta N_m F_2$ values around WSA region (Figure 4), thereby largely contributing to the annual anomaly around midnight. Further, one can observe good spatial correspondence between midnight W_{eff} in Figure 8c and the $\Delta N_m F_2$ values around midnight in Figure 4 indicating that the role of W_{eff} in the presence of geomagnetic field configuration is the main factor responsible for ionospheric annual anomaly. Through case-controlled model simulations, *Zeng et al*. [2008] identified that the offset between geomagnetic center and geographic center is the important factor for annual anomaly in F_2 layer and the tilt of geomagnetic dipole is responsible for its longitudinal variation. However, *Zeng et al*. [2008] have not explained the physical mechanisms about how the offset between geomagnetic center and geographic center causes annual anomaly and did not discussed about the role of neutral winds. In this paper, we have further investigated about how the neutral winds in the presence of geomagnetic field configuration cause annual anomaly during both daytime and nighttime and its latitudinal and longitudinal variability [sections 4.1–4.3].

The $h_m F_2$ and effective neutral wind (W_{eff}) variations presented in Figures 7 and 8 generally explain the important features of ionospheric annual anomaly observed from the $\Delta N_m F_2$ variations in Figure 4, such as

(i) dominant southern hemispheric contribution during both daytime and nighttime, (ii) enhanced ΔN_mF_2 values at southern low latitudes during noon and afternoon hours, (iii) significant enhancements in ΔN_mF_2 around WSA region during nighttime, and (iv) negative ΔN_mF_2 values in the Northern Hemisphere during nighttimes. However, there are still some features which cannot be fully explained by the W_{eff}, such as stronger southern EIA crests during June at noon (12 LT) (Figures 5b and 6b) and enhanced southern EIA crest at 90°W longitude (Figure 6a) where the geomagnetic equator is south of the geomagnetic equator. As discussed earlier, the ionization around EIA latitudes during solstices is largely controlled by the interaction between transequatorial neutral winds and equatorial fountain process. It may be speculated that the seasonal and longitudinal variations in the zonal electric field (strength of equatorial fountain process), probably, are responsible for the observed discrepancies. For example, *Dang et al.* [2017] have shown that the plasma fountain can also be modulated by Sun-Earth distance and contribute to the annual anomaly. Further, *Liu et al.* [2009] have shown that the concentration of atomic oxygen [O] is substantially higher during December than in June solstices, particularly in Southern Hemisphere, which can partly contribute to the annual anomaly in Southern Hemisphere. More modeling efforts with accurate inputs of neutral composition, zonal electric field, and neutral winds are necessary to explain these features.

Finally, it should be noted that the winter anomaly is almost absent at midlatitudes at all local times during this low solar activity year 2009 (Figure 2). The winter anomaly is the condition where the daytime N_mF_2 is greater in the winter hemisphere than in summer hemisphere during solstices. The winter anomaly will be coherent with annual anomaly in the Northern Hemisphere where the northern winter occurs in December solstices, hence, complementing each other. Whereas the winter anomaly generally counterbalances the annual anomaly in the Southern Hemisphere where the southern winter occurs in June solstices, particularly, during high solar activity periods [*Burns et al.* 2014]. However, the absence of winter anomaly during the present low solar activity year 2009 made it possible to observe the southern hemispheric dominance in annual anomaly. Obviously, further studies are required to investigate the southern hemispheric contribution to annual anomaly at high solar activity levels.

5. Conclusions

A detailed study on the ionospheric annual anomaly and its local time, latitudinal, and longitudinal variability is carried out using the F_2 layer peak density (N_mF_2) data from Formosat-3/COSMIC radio occultation observations during the low solar activity year 2009, and the responsible physical mechanisms were investigated. The results consistently indicate that the annual anomaly occurs predominantly at Southern Hemisphere at all local times with significant enhancements at southern EIA crest latitudes during noon to afternoon hours and around Weddell Sea Anomaly region during nighttimes. The possible mechanisms are discussed in terms of effective upward neutral winds due to the geomagnetic field configuration and the interplay between the transequatorial neutral winds and equatorial fountain process. The field-aligned transport of plasma due to upward W_{eff} is more pronounced in southern low latitudes during December due to higher inclination angle of field lines around subsolar point over large portion of globe where the geomagnetic equator is located in northern geographic latitudes as well as at longitudes with westward magnetic declination. This leads to the significantly elevated F_2 layer (increased h_mF_2 values) around southern low latitudes and formation of stronger EIA crests in Southern Hemisphere during the December solstice. This wind-driven upward transport process could be responsible for significantly enhanced annual anomaly at southern EIA crest latitudes during noon and afternoon hours. The enhanced h_mF_2 and stronger EIA crests in the summer hemisphere persist even after the sunset (assisted by equatorward wind) extending the annual anomaly at equatorial and low latitudes into nighttimes (Figure 4). The Weddell Sea Anomaly (WSA) also caused by large effective upward winds, and large declination angles of field lines [*Lin et al.* 2009; *H. Liu et al.* 2010] positively contribute to the annual anomaly during nighttimes in Southern Hemisphere. On the other hand, the annual anomaly occurs only during the production dominant hours of 08–14 LT in the Northern Hemisphere with relatively smaller magnitudes. The annual anomaly is almost absent at other local times in the Northern Hemisphere. This study reveals the role of effective upward winds and the southern summer hemispheric contribution to the ionospheric annual anomaly and provides important insights to physical mechanisms responsible for its local time, latitude, and longitudinal variability.

References

Abdu, M. A., J. H. A. Sobral, G. O. Walker, B. M. Reddy, and B. G. Fejer (1990), Electric field versus neutral wind control of the equatorial anomaly under quiet and disturbed condition: A global perspective from SUNDIAL 86, *Ann. Geophys.*, 8, 419–430.

Anderson, D. N. (1981), Modeling the ambient, low-latitude, F region ionosphere: A review, *J. Atmos. Terr. Phys.*, 43, 753–762, doi:10.1016/0021-9169(81)90051-9.

Bailey, G. J., N. Balan, and Y. Z. Su (1997), The Sheffield University plasmasphere-ionosphere model: A review, *J. Atmos. Sol. Terr. Phys.*, 59, 1541–1552, doi:10.1016/S1364-6826(96)00155-1.

Balan, N., Y. Otsuka, G. J. Bailey, S. Fukao, and M. A. Abdu (2000), Annual variations of the ionosphere: A review based on the MU radar observations, *Adv. Space Res.*, 25, 153–162.

Balan, N., P. K. Rajesh, S. Sripathi, S. Tulasiram, J. Y. Liu, and G. J. Bailey (2013), Modeling and observations of the north-south ionospheric asymmetry at low latitudes at long deep solar minimum, *Adv. Space Res.*, 52, 375–382, doi:10.1016/j.asr.2013.04.003.

Bellchambers, W. H., and W. R. Piggott (1958), Ionospheric measurements made at Halley Bay, *Nature*, 182, 1596–1597, doi:10.1038/1821596a0.

Berkner, L. V., and H. W. Wells (1938), Non-seasonal change of F_2 region ion density, *Terr. Magn. Atmos. Electr.*, 43, 15–36.

Burns, A. G., W. Wang, L. Qian, S. C. Solomon, Y. Zhang, L. J. Paxton, and X. Yue (2014), On the solar cycle variation of the winter anomaly, *J. Geophys. Res. Space Phys.*, 119, 4938–4949, doi:10.1002/2013JA019552.

Chen, C. H., J. D. Huba, A. Saito, C. H. Lin, and J. Y. Liu (2011), Theoretical study of the ionospheric Weddell Sea Anomaly using SAMI2, *J. Geophys. Res.*, 116, A04305, doi:10.1029/2010JA015573.

Dang, T., W. Wang, A. Burns, X. Dou, W. Wan, and J. Lei (2017), Simulations of the ionospheric annual asymmetry: Sun-Earth distance effect, *J. Geophys. Res. Space Physics*, 122, 6727–6736, doi:10.1002/2017JA024188.

Drob, D. P., et al. (2015), An update to the Horizontal Wind Model (HWM): The quiet time thermosphere, *Earth Space Sci.*, 2, 301–319, doi:10.1002/2014EA000089.

Dudeney, J. R., and W. R. Piggot (1978), Antarctic ionospheric research, in *Upper Atmosphere Research in Antarctica, Ant. Res. Ser*, edited by L. J. Lanzerotti and C. G. Park, pp. 200–235, AGU, Washington, D. C.

He, M., L. Liu, W. Wan, B. Ning, B. Zhao, J. Wen, X. Yue, and H. Le (2009), A study of the Weddell Sea Anomaly observed by FORMOSAT-3/COSMIC, *J. Geophys. Res.*, 114, A12309, doi:10.1029/2009JA014175.

Immel, T. J., E. Sagawa, S. L. England, S. B. Henderson, M. E. Hagan, S. B. Mende, H. U. Frey, C. M. Swenson, and L. J. Paxton (2006), Control of equatorial ionospheric morphology by atmospheric tides, *Geophys. Res. Lett.*, 33, L15108, doi:10.1029/2006GL026161.

Johnson, F. S. (1964), Composition changes in the upper atmosphere, in *Electron Density Distributions in the Ionosphere and Exosphere*, edited by E. Thrane, pp. 81–84, North Holland, Amsterdam.

Lei, J., S. Syndergaard, and A. G. Burns (2007), Comparison of COSMIC ionospheric measurements with ground-based observations and model predictions: Preliminary results, *J. Geophys. Res.*, 112, A07308, doi:10.1029/2006JA012240.

Li, X., and T. Yu (2003), Annual and semi-annual variations of the observed f_oF_2 in a high solar activity year, *Terr. Atmos. Ocean. Sci.*, 14(1), 41–62.

Lin, C. H., J. Y. Liu, T. W. Fang, P. Y. Chang, H. F. Tsai, C. H. Chen, and C. C. Hsiao (2007a), Motions of the equatorial ionization anomaly crests imaged by FORMOSAT-3/COSMIC, *Geophys. Res. Lett.*, 34, L19101, doi:10.1029/2007GL030741.

Lin, C. H., W. Wang, M. E. Hagan, C. C. Hiao, T. J. Immel, M. L. Hsu, J. Y. Liu, L. J. Paxton, T. W. Fang, and C. H. Liu (2007b), Plausible effect of atmospheric tides on the equatorial ionosphere observed by the FORMOSAT-3/COSMIC: Three-dimensional electron density structures, *Geophys. Res. Lett.*, 34, L11112, doi:10.1029/2007GL029265.

Lin, C. H., J. Y. Liu, C. Z. Cheng, C. H. Chen, C. H. Liu, W. Wang, A. G. Burns, and J. Lei (2009), Three dimensional ionospheric electron density structure of the Weddell Sea Anomaly, *J. Geophys. Res.*, 114, A02312, doi:10.1029/2008JA013455.

Lin, C. H., C. H. Liu, J. Y. Liu, C. H. Chen, A. G. Burns, and W. Wang (2010), Midlatitude summer nighttime anomaly of the ionospheric electron density observed by FORMOSAT-3/COSMIC, *J. Geophys. Res.*, 115, A03308, doi:10.1029/2009JA014084.

Liu, H., S. V. Thampi, and M. Yamamoto (2010), Phase reversal of the diurnal cycle in the midlatitude ionosphere, *J. Geophys. Res.*, 115, A01305, doi:10.1029/2009JA014689.

Liu, L., B. Zhao, W. Wan, B. Ning, M.-L. Zhang, and M. He (2009), Seasonal variations of the ionospheric electron densities retrieved from Constellation Observing System for Meteorology, Ionosphere, and Climate mission radio occultation measurements, *J. Geophys. Res.*, 114, A02302, doi:10.1029/2008JA013819.

Liu, L., B. Zhao, W. Wan, S. Venkartraman, M.-L. Zhang, and X. Yue (2007), Yearly variations of global plasma densities in the topside ionosphere at middle and low latitudes, *J. Geophys. Res.*, 112, A07303, doi:10.1029/2007JA012283.

Liu, L., M. He, X. Yue, B. Ning, and W. Wan (2010), Ionosphere around equinoxes during low solar activity, *J. Geophys. Res.*, 115, A09307, doi:10.1029/2010JA015318.

Ma, R., J. Xu, and H. Liao (2003), The features and a possible mechanism of semiannual variation in the peak electron density of the low latitude F_2 layer, *J. Atmos. Sol. Terr. Phys.*, 65, 47–57.

Mayr, H. G., and K. K. Mahajan (1971), Seasonal variation in the F_2 region, *J. Geophys. Res.*, 76(4), 1017–1027.

Mendillo, M., C.-L. Huang, X. Pi, H. Rishbeth, and R. Meier (2005), The global ionospheric asymmetry in total electron content, *J. Atmos Sol. Terr. Phys.*, 67, 1377–1387.

Millward, G. H., H. Rishbeth, T. J. Fuller-Rowell, A. D. Aylward, S. Quegan, and R. J. Moffett (1996), Ionospheric F_2 layer seasonal and semiannual variation, *J. Geophys. Res.*, 101, 5149–5156.

Moffet, R. J. (1979), The equatorial anomaly in the electron distribution of terrestrial F region, *Fundam. Cosmic Phys.*, 4, 313–391.

Penndorf, R. (1965), The average ionospheric conditions over the Antarctic, in *Geomagnetism and Aeronomy, Ant. Res. Ser.*, vol. 4, edited by A. H. Waynick, pp. 1–45, AGU, Washington, D. C.

Raghavarao, R., M. Nageswararao, J. H. Sastri, G. D. Vyas, and M. Sriramarao (1988), Role of equatorial ionization anomaly in the initiation of equatorial spread-F, *J. Geophys. Res.*, 93, 5959–5964, doi:10.1029/JA093iA06p05959.

Rajaram, G. (1977), Structure of the equatorial F region, topside and bottomside: A review, *J. Atmos. Terr. Phys.*, 39, 1125–1144, doi:10.1016/0021-9169(77)90021-6.

Rastogi, R. G., and J. A. Klobuchar (1990), Ionospheric electron content within the equatorial F_2 layer anomaly belt, *J. Geophys. Res.*, 95, 19,045–19,052, doi:10.1029/JA095iA11p19045.

Rishbeth, H. (2000), The equatorial F-layer: Progress and puzzles, *Ann. Geophys.*, 18, 730–739, doi:10.1007/s00585-000-0730-6.

Rishbeth, H., and I. C. F. Muller-Wodarg (2006), Why is there more ionosphere in January than in July? The annual asymmetry in the F_2-layer, *Ann. Geophys.*, 24, 3293–3311.

Rishbeth, H., and C. S. G. K. Setty (1961), The F-layer at sunrise, *J. Atmos. Sol. Terr. Phys.*, 21, 263–276.

Sagawa, E., T. J. Immel, H. U. Frey, and S. B. Mende (2005), Longitudinal structure of the equatorial anomaly in the nighttime ionosphere observed by IMAGE/FUV, *J. Geophys. Res.*, *110*, A11302, doi:10.1029/2004JA010848.

Sai Gowtam, V. and S. Tulasi Ram (2017), Ionospheric winter anomaly and annual anomaly observed from Formosat-3/COSMIC Radio Occultation observations during the ascending phase of solar cycle 24, *Adv. Space Res.*, doi:10.1016/j.asr.2017.03.017.

Schreiner, W. S., C. Rocken, S. Sokolovskiy, S. Syndergaard, and D. C. Hunt (2007), Estimates of the precision of GPS radio occultations from the COSMIC/FORMOSAT-3 mission, *Geophys. Res. Lett.*, *34*, L04808, doi:10.1029/2006GL027557.

Sharma, P., and R. Raghavarao (1989), Simultaneous occurrence of ionization ledge and counter electrojet in the equatorial ionosphere: Observational evidence and its implications, *Can. J. Phys.*, *67*, 166–172.

Stening, R. J. (1992), Modeling the low-latitude F region, *J. Atmos. Terr. Phys.*, *54*, 1387–1412, doi:10.1016/0021-9169(92)90147-D.

Su, Y. Z., G. J. Bailey, and K. I. Oyama (1998), Annual and seasonal variations in the low-latitude topside ionosphere, *Ann. Geophys.*, *16*, 974–985.

Thampi, S., C. H. Lin, H. Liu, and M. Yamamoto (2009), First tomographic observations of the Midlatitudes Summer Night Anomaly over Japan, *J. Geophys. Res.*, *114*, A10318, doi:10.1029/2009JA014439.

Titheridge, J. E. (1995), Winds in the ionosphere—A review, *J. Atmos. Terr. Phys.*, *57*, 1681–1714.

Torr, M. R., and D. G. Torr (1973), The seasonal behavior of the F_2-layer of the ionosphere, *J. Atmos. Solar Terr. Phys.*, *35*(12), 2237–2251.

Tulasi Ram, S., S.-Y. Su, and C. H. Liu (2009), FORMOSAT-3/COSMIC observations of seasonal and longitudinal variations of equatorial ionization anomaly and its interhemispheric asymmetry during the solar minimum period, *J. Geophys. Res.*, *114*, A06311, doi:10.1029/2008JA013880.

Volland, H. (1969), The upper atmosphere as a multiple refractive medium for neutral air motions, *J. Atmos. Solar Terr. Phys.*, *31*, 491–514.

Walker, G. O. (1981), Longitudinal structure of the equatorial ionization anomaly: A review, *J. Atmos. Terr. Phys.*, *43*, 763–775, doi:10.1016/0021-9169(81)90052-0.

Walker, G. O., J. H. K. Ma, and E. Gotton (1994), The equatorial ionosphere anomaly in electron content for solar maximum to solar minimum to solar maximum at South East Asia, *Ann. Geophys.*, *12*, 195–209.

Yang, K. F., Y. H. Chu, C. L. Su, H. T. Ko, and C. Y. Wang (2009), An examination of FORMOSAT-3/COSMIC ionospheric electron density profile: Data quality criteria and comparisons with the IRI model, *Terr. Atmos. Ocean. Sci.*, *20*, 193–206 doi:10.3319/TAO.2007.10.05.01 (F3C).

Yonezawa, T. (1971), The solar-activity and latitudinal characteristics of the seasonal, non-seasonal and semi-annual variations in the peak electron densities of the F_2-layer at noon and at midnight in middle and low latitudes, *J. Atmos. Sol. Terr. Phys.*, *33*, 887–907.

Zeng, Z., A. Burns, W. Wang, J. Lei, S. Solomon, S. Syndergaard, L. Qian, and Y.-H. Kuo (2008), Ionospheric annual asymmetry observed by the COSMIC radio occultation measurements and simulated by the TIEGCM, *J. Geophys. Res.*, *113*, A07305, doi:10.1029/2007JA012897.

Zhao, B., W. Wan, L. Liu, T. Mao, Z. Ren, M. Wang, and A. B. Christensen (2007), Features of annual and semiannual variations derived from the global ionospheric maps of total electron content, *Ann. Geophys.*, *25*, 2513–2527, doi:10.5194/angeo-25-2513-2007.